

Phase diagram of the one dimensional Hubbard-Holstein Model at 1/2 and 1/4 filling

R.P. Hardikar and R.T. Clay^{1,*}

¹Department of Physics and Astronomy and HPC² Center for Computational Sciences,
Mississippi State University, Mississippi State MS 39762

(Dated: October 19, 2019)

The Hubbard-Holstein model is one of the simplest to incorporate both electron-electron and electron-phonon interactions. In one dimension at half filling, the Holstein electron-phonon coupling promotes onsite pairs of electrons and a Peierls charge density wave, while the Hubbard onsite Coulomb repulsion U promotes antiferromagnetic correlations and a Mott insulating state. Recent numerical studies have shown that when the two interactions are closely balanced a third intermediate metallic phase emerges. From direct calculations of charge and spin susceptibilities, we show that (i) as the electron-phonon coupling is increased, first a spin gap opens, followed by the Peierls transition, (ii) the transitions between Mott/intermediate and intermediate/Peierls states are of the Kosterlitz-Thouless form, and (iii) for larger U , the two transitions merge at a critical point into a single first order Mott/Peierls transition. In addition we show that an intermediate phase also occurs in the quarter-filled model. The properties of the intermediate phase are similar to the negative- U Hubbard model, with a spin gap but no charge gap.

PACS numbers: 71.10.Fd, 71.30.+h, 71.45.Lr

I. INTRODUCTION

In crystalline materials where one or more of the building blocks of the crystal structure is a large molecule, the vibrational properties of the molecules often have large effects on the overall electronic properties of the material. One large family of such molecular crystalline materials are the organic conductors and superconductors¹. While some molecular crystals such as the fullerene superconductors² have a three-dimensional crystal structure, many other examples are either quasi-one or quasi-two dimensional, *i.e.* charge transport is restricted in certain directions due to anisotropic crystal structure. In addition to strong electron-phonon (e-ph) coupling to the molecular vibrations, electron-electron (e-e) interactions are often important in low dimensional materials. In this paper, we present numerical calculations of the phase diagram for one of the simplest possible many-body models incorporating both these effects, the Hubbard-Holstein model (HHM) in one dimension (1D). In the HHM, internal (intra-molecular) molecular vibrations are coupled to the local charge density of the electrons³. The electrons further interact with other electrons with an on-site Coulomb repulsion when two electrons occupy the same orbital⁴. We will show that surprisingly interesting physics results from this simple model due to the combined effects of both e-e and e-ph interactions.

The 1D HHM Hamiltonian we consider is

$$H = -t \sum_{j,\sigma} (c_{j+1,\sigma}^\dagger c_{j,\sigma} + h.c.) + U \sum_j n_{j,\uparrow} n_{j,\downarrow} + g \sum_{j,\sigma} (a_j^\dagger + a_j) n_{j,\sigma} + \omega \sum_j a_j^\dagger a_j, \quad (1)$$

where $c_{j,\sigma}^\dagger$ ($c_{j,\sigma}$) are creation (annihilation) operators for electrons on site j with spin σ , a_j^\dagger (a_j) are bosonic creation (annihilation) operators for phonons at site j , and

the electron number operator $n_{j,\sigma} = c_{j,\sigma}^\dagger c_{j,\sigma}$. U is the Hubbard onsite e-e interaction energy, ω is the dispersionless phonon frequency, and g is the e-ph coupling constant. All energies in this paper will be given in units of t , the electron hopping integral.

We will concentrate primarily on Eq.1 in the 1/2-filled band limit (one electron per lattice site), but also discuss briefly the 1/4 filled band (one electron per two lattice sites). The effect of e-ph interactions on a 1/2-filled 1D metal is well known: for inter-molecular phonons corresponding to the relative motion of adjacent molecules in the crystal, the 1D lattice dimerizes with alternating strong and weak bonds. In this bond-order wave (BOW) state the expectation value of the electron hopping between adjacent sites alternates between strong and weak values. The dimerized chain then has a gap at the Fermi level and an insulating ground state⁵. This Peierls state has both charge and spin gaps, and a bond modulation at $2k_F$ ($q = \pi$) at 1/2 filling. For Holstein-type phonons that couple to the local charge density, a similar Peierls state occurs, but instead of bond deformation the local charge density is modulated in a charge density wave (CDW) ground state. The CDW Peierls state at 1/2 filling has alternating large and small charge densities again with periodicity $2k_F$. Similarly, the effect of the Hubbard onsite interaction in 1D is well known: for any $U > 0$ at 1/2 filling, the ground state is an insulator⁶. Anti-ferromagnetic (AFM) spin correlations are present in this Mott insulating state, although no long-range antiferromagnetic order is possible in 1D.

At 1/2 filling, the $2k_F$ CDW cannot coexist with $2k_F$ AFM correlations, and it was first thought that in the 1/2 filled HHM there is a single transition between Mott and Peierls states^{7,8}. This simple interpretation is complicated by quantum fluctuations of the phonons which may destroy the Peierls order. A metallic phase was found for $U = 0$ below a critical e-ph coupling^{9,10}, and

was also proposed to exist between Mott and Peierls states¹¹. Subsequent numerical calculations confirmed that a metallic phase exists for both $U = 0$ and finite U ¹². In this paper, we confirm the intermediate phase, and present more detailed analysis of the quantum phase transitions. From finite-size analysis, we determine that the two transitions (Mott/intermediate and intermediate/Peierls) are of the Kosterlitz-Thouless (KT) type. We find that for larger U , the two transitions merge into a single first-order Mott/Peierls transition. We present the phase diagram for three different phonon frequencies. We further show that at 1/4 filling a similar intermediate phase occurs.

The outline of the paper follows. We first give some details of the numerical method we used. Turning to our results, we discuss the $U = 0$ case and then move on to finite U and the 1/4 filled band. Finally, we conclude with a discussion of our data and their relation to other theoretical results, as well as unanswered questions for further study.

II. METHOD

We use the Stochastic Series Expansion (SSE) quantum Monte Carlo method^{13,14,15,16,17}. SSE provides statistically exact results (no Trotter discretization of imaginary time is used) and has been adapted for many different quantum lattice models. Although this method has been described in detail elsewhere, we briefly describe here our treatment of the Holstein phonon interaction.

In SSE, the partition function $Z = \text{Tr}\{e^{-\beta H}\}$ is expanded in terms of a series of sequences S_L of operators H_{a_i, b_i} :

$$Z = \sum_{\alpha} \sum_{S_L} \frac{\beta^n (L-n)!}{L!} \langle \alpha | \prod_{i=1}^L H_{a_i, b_i} | \alpha \rangle \quad (2)$$

In Eq. 2, n is the length (number of operators) of each sequence, L the maximum allowed sequence length, and β is the inverse temperature and $|\alpha\rangle$ is a basis state, here a direct product of electron and phonon configurations. In order to obtain the ground-state phase diagram, all results presented here used $\beta/t \geq 2N$, where N is the number of lattice sites. The operators H_{a_i, b_i} define the Hamiltonian, and have type (a_i) and bond (b_i) indices with i indicating their position within the sequence S_L . For the 1D Hubbard model (Eq. 1 with $g = \omega = 0$), we have three different operators representing the diagonal interaction and electron hopping for both spins¹³:

$$\begin{aligned} H_{1,j} &= C - \frac{U}{2}[(n_{\uparrow,j} - \frac{1}{2})(n_{\downarrow,j} - \frac{1}{2}) \\ &+ (n_{\uparrow,j+1} - \frac{1}{2})(n_{\downarrow,j+1} - \frac{1}{2})] \\ &+ \mu(2 - n_j - n_{j+1}) \end{aligned} \quad (3)$$

$$H_{2,j} = c_{j+1,\uparrow}^\dagger c_{j,\uparrow} + h.c. \quad (4)$$

$$H_{3,j} = c_{j+1,\downarrow}^\dagger c_{j,\downarrow} + h.c. \quad (5)$$

Here j labels the first site of the bond the operator acts on. μ is the chemical potential, written here so that $\mu = 0$ corresponds to 1/2 filling. C is a constant chosen so that the expectation value of $H_{1,j}$ is always positive definite. In addition to the operators of Equations 3—5, a null operator H_0 is used as a place-holder in the sequence expansion. We represent the phonons in the phonon-number basis and add the following operators for the e-ph interactions and phonon diagonal energy:

$$H_{4,j}^L = g a_j^\dagger n_j \quad (6)$$

$$H_{4,j}^R = g a_{j+1}^\dagger n_{j+1} \quad (7)$$

$$H_{5,j}^L = g a_j n_j \quad (8)$$

$$H_{5,j}^R = g a_{j+1} n_{j+1} \quad (9)$$

$$H_{6,j} = \omega(N_p - a_j^\dagger a_j) \quad (10)$$

Additionally, for the HHM, μ in Eq. 3 should be replaced by $(2g^2/\omega + \mu)$. Since the Holstein interaction couples the electron density on a single site while the SSE operators typically act on bonds composed of two sites, we define two different phonon operators acting on phonon numbers on the left or right of the bond. These have superscripts “L” and “R” respectively. The diagonal operator $H_{6,j}$ also acts on a single site j . N_p is a cutoff in the maximum number of phonons per site. We discuss further below the choice of this cutoff, but in practice it can be chosen large enough so as to not affect the accuracy of the method.

The Monte Carlo updating is composed of an update for the electrons followed by an update for the phonons. The electron update consists of an update changing the number of diagonal $H_{1,j}$ operators in the sequence, followed by a loop update that exchanges diagonal and off-diagonal operators. For the electrons we use the directed loop algorithm¹⁷. We note that the operators Eq. 6 through Eq. 10 are not changed during the electron loop update. The phonon updating also consists of two parts, first a diagonal update changing numbers of $H_{6,j}$ operators, and second an off-diagonal update exchanging H_1 , H_4 , and H_5 operators. In the diagonal phonon update, H_0 operators are interchanged with $H_{6,j}$ operators with the following Metropolis algorithm probabilities (N_H is the total number of non- H_0 operators present in the sequence):

$$P_{0 \rightarrow 6} = \frac{N \beta \omega (N_p - \langle a_j^\dagger a_j \rangle)}{L - N_H} \quad (11)$$

$$P_{6 \rightarrow 0} = \frac{L - N_H + 1}{N \beta \omega (N_p - \langle a_j^\dagger a_j \rangle)} \quad (12)$$

The phonon update for off-diagonal operators is similar to the technique described in Reference 18. For each site in the system, a *subsequence* is constructed which is a subset of the operators in S_L . The subsequence consists of only the operators $H_{1,m}$, $H_{4,m}$, and $H_{5,m}$ which act on phonons at a particular site m . Within the subsequence, adjacent pairs of operators are then selected at

random and changed with a Metropolis probability. The pair substitutions that change the phonon number are (omitting the site index m as all apply to the same site):

$$(H_1, H_1) \rightarrow (H_4, H_5), (H_5, H_4) \quad (13)$$

$$(H_4, H_5) \rightarrow (H_1, H_1) \quad (14)$$

$$(H_5, H_4) \rightarrow (H_1, H_1) \quad (15)$$

In addition, pair substitutions are attempted that swap the order in the subsequence of the two operators. When two different pairs may be substituted the substitution made is chosen randomly. Note that the L and R indices in Eq. 6 through Eq. 9 are not needed during the pair updating, but updates involving the H_1 operators must be canceled with 50% probability (for each H_1 operator in the pair). If a H_1 operator changes into a phonon operator as a result of the update, a L or R index is assigned when the subsequence update is completed and merged into S_L . The Metropolis substitution probabilities depend on phonon as well as diagonal electron matrix elements variables, the e-ph coupling constant g , and the number N_d of diagonal phonon operators ($H_{6,j}$) that are present between the two operators of the pair. N_d may be stored when the subsequence is constructed. For example, in terms of just the change in the phonon part of the operator,

$$P[(H_1, H_1) \rightarrow (H_5, H_4)] = Rng^2 \left[\frac{N_p - n + 1}{N_p - n} \right]^{N_d} \quad (16)$$

$$P[(H_5, H_4) \rightarrow (H_1, H_1)] = \frac{R}{ng^2} \left[\frac{N_p - n}{N_p - n + 1} \right]^{N_d} \quad (17)$$

where n is the number of phonons present in the sequence position just before the operator pair. R in Eq. 16 and Eq. 17 is the ratio of diagonal matrix elements from the electronic Hamiltonian. In practice, the number of pair substitutions performed is chosen to be approximately the same as the number of operators in the subsequence.

We use standard methods to calculate various observables within our SSE code¹³. To determine phase boundaries of the model we primarily use the charge and spin susceptibilities at wavevector q given by

$$O_j^\pm = n_{j,\uparrow} \pm n_{j,\downarrow} \quad (18)$$

$$\chi_{\rho,\sigma}(q) = \frac{1}{N} \sum_{j,k} e^{iq(j-k)} \int_0^\beta d\tau \langle O_j^\pm(\tau) O_k^\pm(0) \rangle \quad (19)$$

In Eq. 19 the charge susceptibility $\chi_\rho(q)$ (spin susceptibility $\chi_\sigma(q)$) corresponds to the + (−) sign. Similarly, we also use the static structure factors, $S_\rho(q)$ and $S_\sigma(q)$:

$$S_{\rho,\sigma} = \frac{1}{N} \sum_{j,k} e^{iq(j-k)} \langle O_j^\pm O_k^\pm \rangle \quad (20)$$

All results presented here used the quantum parallel tempering method on a parallel computer¹⁹.

The effective low-energy properties of many interacting 1D models can be understood in terms of a Luttinger

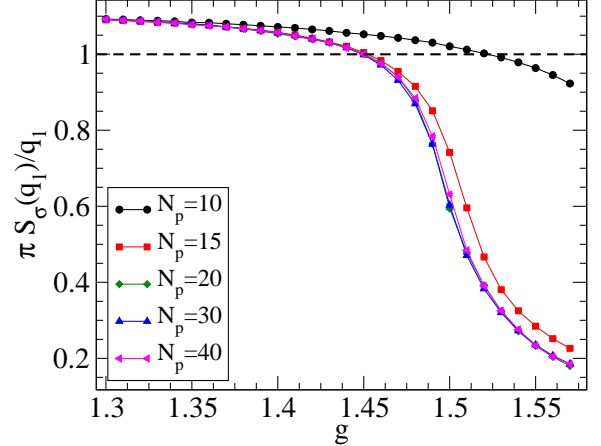


FIG. 1: (color online) Slope of the spin structure factor at wavevector $q_1 = 2\pi/N$ versus e-ph coupling g for a 16 site 1/2 filled system with $U = 4$ and $\omega = 1$. $\pi S_\sigma(q_1)/q_1$ crossing one indicates the opening a spin gap. Different symbols show the convergence with increasing phonon cutoff N_p .

Liquid (LL) picture, and the asymptotic properties of the system described by a small number of parameters^{20,21}. In particular, the asymptotic decay of correlation functions can be related to the correlation exponents K_ρ and K_σ for charge and spin respectively. In the long wavelength limit, these exponents may be calculated from the slope of the structure factors:

$$K_{\rho,\sigma} = \pi \lim_{q \rightarrow 0} S_{\rho,\sigma}(q)/q \quad (21)$$

In practice, one uses the behavior of $\pi S(q)/q$ at the smallest available q for the periodic ring, $q_1 = 2\pi/N$. With proper finite-size scaling in N , this gives the Luttinger liquid exponent for the system²². Based on calculations of acoustic phonons coupled to 1D electrons it has been suggested that the expected relationship of K_ρ to the correlation functions must be modified in the presence of phonon interactions with retardation^{23,24,25}. We will discuss this further in Section III D below. However, we note that the interpretation of K_σ is *not* modified in the presence of phonon retardation effects since spin-rotation symmetry is preserved in the HHM. K_σ is expected to be exactly equal to one unless a spin gap is present, and the condition that $\pi S_\sigma(q_1)/q_1$ decreases below one is a sensitive indicator for the opening of a spin gap (see Fig. 1)¹⁶. We find that finite-size effects in determining the phase boundaries using Eq. 21 are worse than when using the susceptibilities, Eq. 19, due to the necessity of taking the limit $q_1 \rightarrow 0$ in Eq. 21. Therefore we will primarily use the susceptibilities in order to determine the phase diagram boundaries.

We choose the phonon cutoff N_p such that phonon occupation numbers during the simulation never reach within some fraction ($\sim 20\%$) of the cutoff, similar to the method in which the maximum sequence length L is set self-consistently in SSE simulations. We have verified

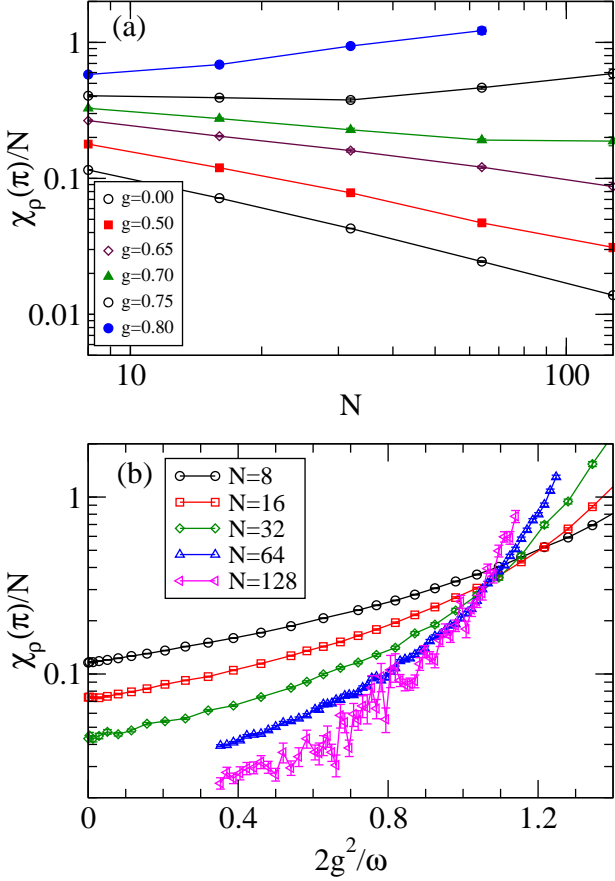


FIG. 2: (color online) Finite-size scaling of the $q = \pi$ charge susceptibility for $U = 0$ and $\omega = 1$ at 1/2 filling. Data are for system sizes up to $N = 128$ sites. In (a) we plot $\chi_\rho(\pi)/N$ versus N . At critical coupling $\chi_\rho(\pi)/N$ approaches a constant for large N . Note that the $g = 0$ curve corresponds to free fermions (no phonons). In (b) $\chi_\rho(\pi)/N$ is plotted versus the effective e-ph coupling $2g/\omega$. We estimate the critical coupling as $2g_{c2}^2/\omega \approx 1.0$ ($g_{c2} \approx 0.71$).

that our results are converged with respect to N_p . Typical variation with N_p is shown in Fig. 1 for a 16 site system with $U = 4$ and $\omega = 1$. We find that choosing N_p too small can have a noticeable effect on the critical coupling for transitions, and especially on quantities measured in the Peierls phase.

III. RESULTS AT HALF-FILLING

We first present our results for the 1/2 filled band, first in the case $U = 0$ and then for finite U .

A. $U = 0$: the Peierls transition

Eq. 1 has been studied in great detail for the case of $U = 0$. One of the key questions is whether the transition to the Peierls state occurs for finite critical coupling or

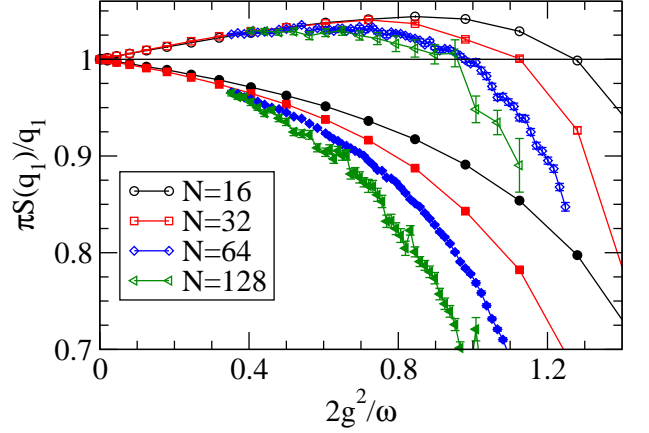


FIG. 3: (color online) Long-wavelength spin and charge structure factor slopes for $U = 0$ and $\omega = 1$ at 1/2 filling. Open (filled) symbols are for charge (spin). Data are for system sizes up to $N = 128$ sites. For any $g > 0$ $\pi S_\sigma(q_1)/q_1$ is less than 1 indicating the presence of a spin gap. The appearance of these data for $g < g_{c2}$ are similar to those for the negative U Hubbard model (Fig. 6 for $U < 0$). The interpretation of these data is discussed in Section III D.

for any value of $g > 0$. The transition occurring at finite g is expected to be of the KT type^{7,26}. KT transitions at finite phonon coupling have been found in a number of 1D phonon-coupled models including the spinless Holstein model (Eq. 1 with only one species of fermion)^{7,27}, the XY model coupled to dispersionless phonons²⁸, the Heisenberg model coupled to dispersionless phonons¹⁵, and the extended Peierls-Hubbard model coupled to dispersionless bond phonons¹⁶. For the Holstein Hamiltonian for spin- $\frac{1}{2}$ electrons we consider, early predictions were that while the spinless model required a finite g for the Peierls state, the model with spin was in the Peierls state for any nonzero g ⁷. However, more recent studies found that a finite coupling is required^{9,10,12}. We confirm that indeed a finite critical coupling exists and show that the finite-size scaling of the observables is consistent with a KT transition.

A KT quantum phase transition is difficult to detect because the gap opens exponentially slowly. For Holstein-type phonons that couple to the local electron density, the appropriate order parameter for the transition is the $2k_F$ charge susceptibility. The critical coupling (we will denote the critical g for the Peierls transition as g_{c2}) may be determined from the finite-size scaling of the $2k_F$ charge susceptibility, $\chi_\rho(\pi)$. $\chi_\rho(\pi)/N$ should approach zero logarithmically below g_{c2} and should diverge above g_{c2} . Exactly at $g = g_{c2}$, log corrections vanish and $\chi_\rho(\pi)/N$ should approach a constant value with increasing N . Our SSE results confirm that $\chi_\rho(\pi)$ does scale in this manner. In Fig. 2(a) we show charge susceptibility data for $U = 0$ and $\omega = 1$, which is consistent with a KT transition at $g_{c2} \approx 0.7$. We see a clear decrease of $\chi_\rho(\pi)/N$ with system size below the transition and a clear increase above the transition. Plotted as a function

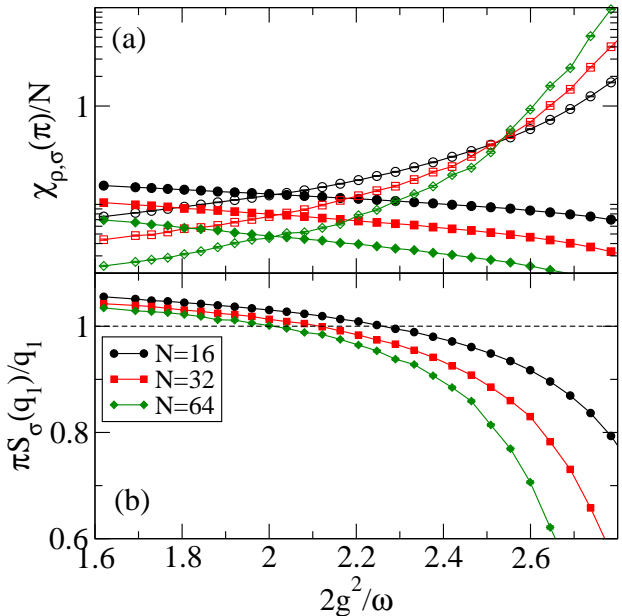


FIG. 4: (color online) (a) Charge (open symbols) and spin (filled symbols) susceptibility for the 1/2 filled HHM with $U = 2$, $\omega = 1$. The first transition (g_{c1}) occurs where $\chi_\rho = \chi_\sigma$, corresponding to $U_{\text{eff}} = 0$. The second transition (g_{c2}) is the Peierls transition, where $\chi_\rho(\pi)/N$ diverges as in Fig. 2. Note that the spin susceptibility is also divided by N to make the crossing at $U_{\text{eff}} = 0$ clear. (b) Long-wavelength spin structure factor for $U = 2$, $\omega = 1$. The point where $\pi S_\sigma(q_1)/q_1$ crosses unity indicates the opening of the spin gap, identical to the point where $\chi_\rho = \chi_\sigma$ in (a).

of effective e-ph coupling $2g^2/\omega$ (Fig. 2(b)), $\chi_\rho(\pi)/N$ for different N cross at the transition.

In Fig. 3 we show for comparison the long-wavelength charge and spin structure factor slopes, Eq. 21, which are estimates for the LL exponents K_ρ and K_σ . For any $g > 0$ K_σ is less than 1 and decreases with increasing chain length, indicating a spin gap. Furthermore, in the spin susceptibility (not shown here), we find no sign of any transition at the critical coupling where $\chi_\rho(\pi)/N$ diverges. We denote the critical coupling for the spin gap opening as g_{c1} . Hence we conclude that a spin gap is present for *any* $g > g_{c1} = 0$ when $U = 0$, but a charge gap is only present for $g > g_{c2}$. We discuss further the K_ρ data in Section III D.

B. $U > 0$: Intermediate phase

We next consider the case with $U > 0$ at 1/2 filling. To avoid any possible difficulties of interpreting numerical estimates for K_ρ , we determine all phase boundaries *directly from susceptibilities* and K_σ . In the 1D Hubbard model ($g = 0$ in Eq. 1) charge and spin degrees of freedom effectively switch places at $U = 0$. In terms of the susceptibilities, $\chi_\rho(\pi)$ and $\chi_\sigma(\pi)$ are exactly equal at $U = 0$.

Turning to the HHM, in the limit $\omega \rightarrow \infty$ one can integrate out the phonons leaving an effective attractive interaction. We now have an effective U composed of the sum of the Hubbard U and the effective phonon interaction, $U_{\text{eff}} = U - 2g^2/\omega$. For $U_{\text{eff}} > 0$ we expect the Mott state, while for $U_{\text{eff}} < 0$ it has usually been assumed that the model is in the Peierls state⁷. In Fig. 4(a) we first show the $2k_F$ charge and spin susceptibilities for $U = 2$ and $\omega = 1$. We find that when $U_{\text{eff}} \approx 0$ ($g = 1$ for $U = 2$ and $\omega = 1$), the charge and spin susceptibilities become equal, like the 1D Hubbard model at $U = 0$. We will refer to the critical coupling where $\chi_\rho(2k_F) = \chi_\sigma(2k_F)$ as g_{c1} ¹². The transition at g_{c1} corresponds to the opening of a spin gap, as shown in Fig. 4(b) by the estimate for K_σ , which crosses one at g_{c1} . This first transition as g increases past g_{c1} appears identical to the transition as U becomes negative in the 1D Hubbard model. Based on the similarity with the 1D Hubbard model, we conclude that the spin gap transition here is also of the KT form.

In Fig. 4(a) a second transition takes place beyond the spin gap transition at g_{c1} . This second transition is again the Peierls transition indicated by the divergence of $\chi_\rho(\pi)$. Beyond the second transition point ($g > g_{c2}$) $\chi_\rho(\pi)/N$ increases with increasing system size, and as in Fig. 2(b) $\chi_\rho(\pi)/N$ for different system sizes cross at $g = g_{c2}$ when plotted versus e-ph coupling. For $g_{c1} < g < g_{c2}$ we now have a third intermediate phase, which has a spin gap but no Peierls order. In Fig. 4(a) we see only very small finite-size effects in determining g_{c1} and g_{c2} from the susceptibility data. The g_{c1} from our data shows little deviation from $U_{\text{eff}} = 0$, at least for small to intermediate U as compared to ω . Finite-size effects are more significant in K_σ as estimated from the spin structure factor slope in Fig. 4(b) because $q_1 = 2\pi/N$ only approaches $q_1 = 0$ in the limit $N \rightarrow \infty$. However, for increasing N , g_{c1} as estimated from K_σ does converge to the same value we obtain from the susceptibility. As U increases, we find that two transitions occur closer together, becoming indistinguishable from each other at approximately $U \sim 5$ for $\omega = 1$. At this point and for larger U , the two KT transitions merge into a single Mott/Peierls transition. We next show that this merged transition is *first order*.

C. First order transition

Above a critical U value $U = U_m$ we find that the spin-gap and Peierls transitions coincide. The phase diagram then has a shape very similar to that of the 1/2 filled 1D extended Hubbard model (EHM)^{19,29,30,31}. In the 1/2 filled EHM, as the nearest-neighbor Coulomb repulsion V is increased for fixed U , there is a transition from AFM to CDW order. This transition is continuous for small U and first-order for $U > U_m$. In a first-order quantum phase transition, observables become discontinuous as one of the Hamiltonian parameters is varied. As in Reference 19 we take $[m(\rho)]^2 = S_\rho(\pi)/N$ as an or-

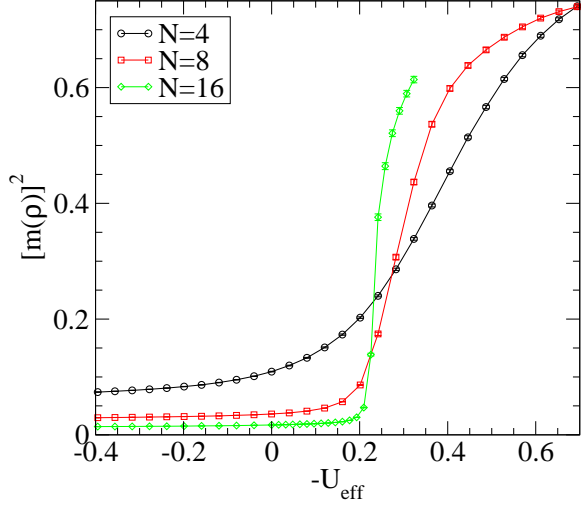


FIG. 5: (color online) First order Mott/Peierls transition for large U . We show the CDW order parameter $[m(\rho)]^2$ (see text) vs. $-U_{\text{eff}} = 2g^2/\omega - U$ for $\omega = 1$ and $U = 8$. The Mott/Peierls transition occurs for $U_{\text{eff}} \sim -0.2$.

der parameter for the Peierls CDW state. We show in Fig. 5 $[m(\rho)]^2$ for $U = 8$ and $\omega = 1$. We find a sharp jump in $[m(\rho)]^2$ at the transition with the discontinuity becoming stronger for larger system sizes. Other observables such as the ground state energy and bond order also show discontinuous behavior consistent with a first order transition. In fact, this point is a *multi-critical* point. In the EHM there is an intervening phase with long-range BOW for $U < U_m$ ^{19,32,33}. We find very similar behavior in the HHM except that the intervening phase here is the metallic intermediate state. We cannot calculate a precise value for U_m , but for $\omega = 1$ it appears comparable ($U_m \sim 5$ for $\omega = 1$) to the value found in the 1/2 filled EHM, $U_m = 4.7 \pm 0.1$ ¹⁹. We also remark that the change in the order of the transition may be related to discussions of quantum to classical crossover in e-ph coupled models³⁴.

D. Discussion of Luttinger exponents

In the LL picture, K_ρ and K_σ determine the asymptotic decay of correlations functions and hence measurements of these exponents in finite systems have often been used to determine the phase diagrams of 1D models. Specifically, $K_\rho > 1$ corresponds to attractive charge correlations, while $K_\rho < 1$ corresponds to repulsive charge correlations. It is first instructive to review the LL exponents for the 1D Hubbard model and sources of error in finite-size systems. At 1/2 filling for $U > 0$ the 1D Hubbard model is insulating ($K_\rho = 0$) with no spin gap ($K_\sigma = 1$, spin rotational invariance holds). For $U < 0$ there is a spin gap ($K_\sigma = 0$), and degenerate CDW and singlet superconducting (SS) pair correlations ($K_\rho = 1$). Therefore, the LL exponents are *discontinuous* at $U = 0$.

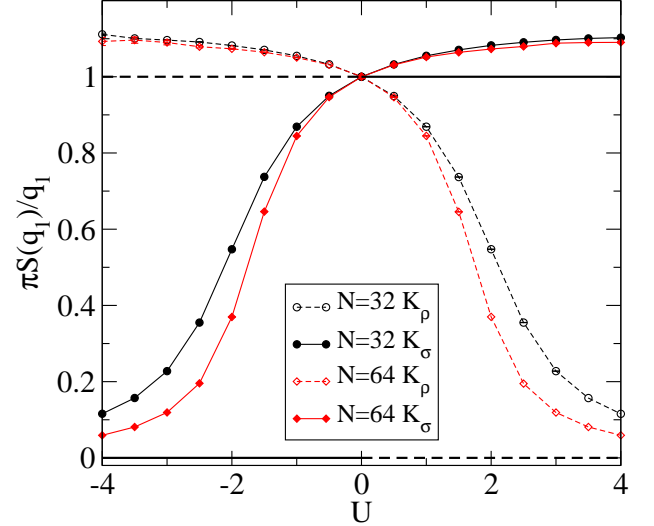


FIG. 6: (color online) LL exponents for the 1D Hubbard model (Eq. 1 with $g = 0$) estimated from the long-wavelength charge and spin correlations. K_ρ (K_σ) is given by open (filled) symbols. In the infinite N limit, $K_\rho = 1$ for any $U < 0$ and $K_\rho = 0$ for $U > 0$; $K_\sigma = 1$ for any $U > 0$ and $K_\sigma = 0$ for any $U < 0$. Observing these limiting values (shown by full and dashed horizontal lines) is difficult due to finite value of $q_l = 2\pi/N$ and also the logarithmic scaling with N for the exponent whose value is unity.

The transition at $U = 0$ is of the KT type, with the gaps (charge gap $U > 0$ or spin gap $U < 0$) opening exponentially slowly as U is varied from zero. In Fig. 6 we show K_ρ and K_σ for the 1D Hubbard model calculated using Eq. 21. There are two primary sources of finite-size error: first, the requirement that $q \rightarrow 0$ in Eq. 21, and second, the presence of logarithmic scaling corrections near a KT transition. The scaling with system size is slow close to the transition ($U = 0$) and particularly slow for the exponent that is expected to be equal to 1 (K_σ for $U > 0$ and K_ρ for $U < 0$). Such logarithmic scaling has been noted in other 1D electron and spin models and makes it difficult in practice to observe $K_\sigma = 1$ for the positive- U Hubbard model in a finite-size calculation^{15,16}. As discussed in Section III A, log corrections are expected to vanish exactly at critical coupling. In Fig. 6 this occurs at $U = 0$, where K_ρ and K_σ curves for all system sizes cross at $K_\rho = K_\sigma = 1$.

Turning now to the HHM, the variation of K_σ for $g < g_{c1}$ (Fig. 4(b)) is consistent with log corrections in the spin degree of freedom that vanish at the spin gap transition. This observation further reinforces our statement that the spin gap transition is also of the KT type. For the K_ρ data in Fig. 3, K_ρ at $g = 0$ is again exactly unity. K_ρ then crosses one from above at a g roughly consistent with the g_{c2} determined from the susceptibility data in Fig. 2. Assuming the Peierls transition occurs where $K_\rho = 1$ gives a critical coupling of $g_{c2} = 0.65 \pm 0.02$ after performing finite-size scaling using N up to 128 sites, very close to our estimate from

the charge susceptibility. The form of the K_ρ plot for the HHM ($U = 0$) is clearly similar to K_ρ for the negative U Hubbard model (Fig. 6), with K_ρ starting at one for zero coupling, and becoming slightly *larger* than one for nonzero coupling. While this apparent $K_\rho > 1$ may be interpreted as meaning that superconducting pair correlations are dominant¹², a more plausible interpretation is that the apparent $K_\rho > 1$ is a consequence of logarithmic scaling corrections. This implies that the true K_ρ should be exactly equal to unity for $g < g_{c2}$, and drop to zero for $g > g_{c2}$. This further implies that the intermediate state has *degenerate* CDW and SS correlations. This statement is consistent with our finding that the $U = 0$ HHM for $g < g_{c2}$ has a spin gap but no charge gap.

Calculations for a model of acoustic phonons coupled to 1D electrons found that the LL expressions for decay of correlation functions must be modified due to retardation effects²³. Specifically, the dominance of CDW and SS correlations is given by

$$K_\rho A \leq 1 \quad (\text{CDW}) \quad (22)$$

$$B/K_\rho \leq 1 \quad (\text{SS}) \quad (23)$$

where A and B depend on the strength of the e-ph coupling²³. With zero e-ph coupling, $A = B = 1$. For increasing e-ph coupling, $A > 1$ and $B < 1$, with A diverging and B approaching a finite value. The renormalized boundary for the metallic/Peierls transition is then $K_\rho = 1/A$. While there is no reason to expect that for the HHM model (with dispersionless phonons) the LL relations should be renormalized in the same manner, our SSE data may be consistent with $1/A$ slightly less than 1. Upon close examination of Fig. 3 and Fig. 2, the g_{c2} as determined by K_ρ crossing one *may* be slightly smaller than the g_{c2} determined by susceptibility. The g_{c2} determined from K_ρ (Fig. 3) would coincide with the g_{c2} determined from $\chi_\rho(\pi)$ (Fig. 2(b)) if the horizontal line in Fig. 3 is moved slightly below one, or $1/A \approx 0.95$.

For larger U , the size of the intermediate region shrinks, and K_ρ peaks at the transition, with K_ρ approaching one with increasing N (see Fig. 2(a) in Reference 12, $U = 2$, $\omega = 0.5$). The peak at the transition is consistent with $K_\rho = 0$ in the Mott and Peierls states, and $K_\rho = 1$ only along their boundary. The apparent $K_\rho < 1$ at the peak may be due to the closer proximity to the first order transition, where K_ρ drops quite rapidly to zero. For $U = 2$ and $\omega = 0.5$, we estimate that $0.95 \lesssim 1/A \leq 1$. We stress that our data and the determination (finite size extrapolation) of g_{c2} are uncertain enough that it is difficult to definitively determine if $A > 1$. However, if renormalization as in Reference 23 does occur, for all parameter values we investigated it appears that the effect is small ($A \approx 1$).

Because measuring SS correlations is not practical in the SSE method, we cannot determine a value for B . Eq. 23 with $B < 1$ would imply that a SS correlations are dominant whenever K_ρ exceeds a value that is *smaller* than one. SS is dominant for any nonzero e-ph coupling for $U = 0$ in the calculation of Reference 23, which seems

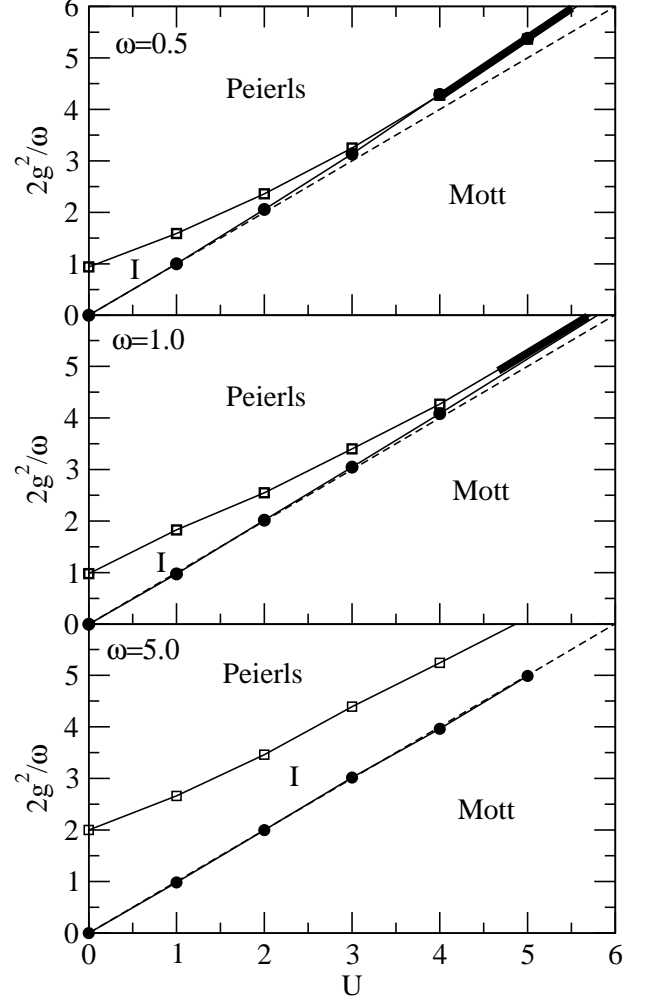


FIG. 7: Phase diagram of the 1/2 filled HHM for $\omega = 0.5$, $\omega = 1$, and $\omega = 5$. The dashed line is given by $U = 2g^2/\omega$. All phase boundaries are determined using susceptibility and K_σ data, with uncertainty approximately the size of the symbols. Lines are guides to the eye. The three phases shown are Mott, (I)ntermediate, and Peierls. The Mott/I and I/Peierls boundaries merge into a single first-order Mott/Peierls boundary indicated by a heavy line for $U \gtrsim 4$ for $\omega = 0.5$ and $U \gtrsim 5$ for $\omega = 1$.

unlikely in the HHM. We will discuss these implications further in Section V.

E. Phase diagram, 1/2 filling

In Fig. 7 we show the phase diagram for $\omega = 0.5$, $\omega = 1$, and $\omega = 5$. All points were determined using susceptibility data for systems up to 32 (and in some cases 64 and 128) sites. We find that with increasing ω the width of the intermediate region increases, and the tricritical point U_m moves to larger U . One further observation is that for $U \gtrsim U_m$, the deviation of the Mott/Peierls boundary from $U_{\text{eff}} = 0$ becomes noticeable, with the

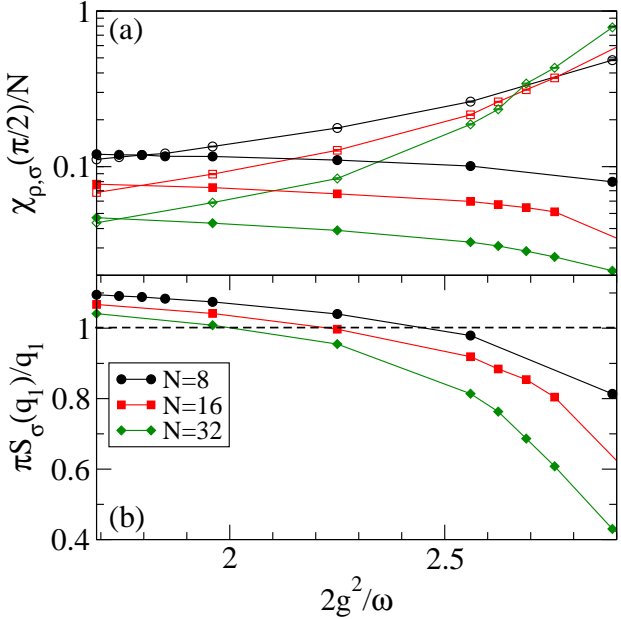


FIG. 8: (color online) (a) Charge (open symbols) and spin (filled symbols) susceptibilities for the quarter filled HHM with $U = 2$, $\omega = 0.5$. (b) Long-wavelength spin structure factor for same parameters. We find similar behavior to 1/2 filling, Fig. 4, with first a transition to a spin-gapped state, and second the transition to the Peierls CDW state.

boundary shifting to $U_{\text{eff}} < 0$ (above the dotted lines in Fig. 7. This shift can be seen for example in Fig. 5. For $U < U_m$, the Mott/Intermediate spin gap boundary is very close to the line $U_{\text{eff}} = 0$.

IV. 1/4 FILLING

Many of the materials that the HHM is most applicable to are not 1/2 filled. For example, most of the quasi-1D organic superconductors are 3/4 filled (1/4 hole filled)¹. We therefore present some results for the HHM at 1/4 filling. Although for many of these materials it is necessary to include long ranged Coulomb interactions (the extended Hubbard V term)³⁵, we will continue to focus on the HHM Hamiltonian with only onsite U and e-ph terms. We comment on the expected effect of V further below. As 1/4 filling is commensurate a Peierls state is also expected to occur for sufficiently large g . There are however significant differences between 1/2 filled and 1/4 filled Peierls states. At 1/4 filling, there is more than one possible pattern of charge and bond distortion, and which one actually occurs depends on the values of U as well as V ^{36,37}. In the absence of phonons, the 1/4-filled band for finite U is a LL with neither charge nor spin gaps. As at 1/2 filling, $\chi_{\rho}(2k_F)$ and $\chi_{\sigma}(2k_F)$ are degenerate at $U = 0$ (note that $2k_F = \pi/2$ at 1/4 filling and corresponds to a correlation function with period 4 in real space). In the presence of phonons, we again expect

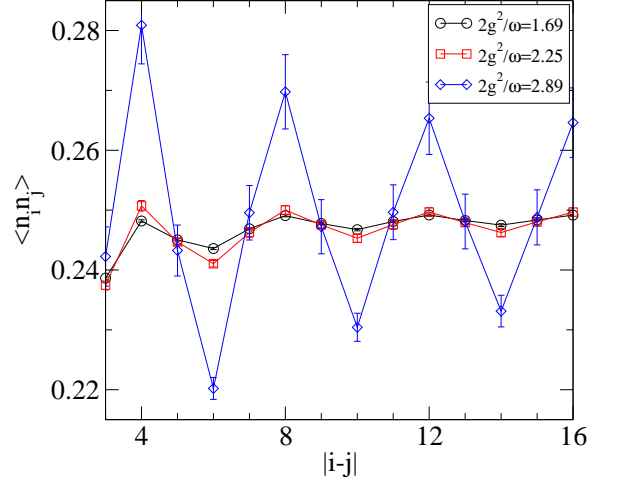


FIG. 9: (color online) Charge-charge correlations $\langle n_i n_j \rangle$ versus distance $|i-j|$ for a 32 site 1/4 filled system with $U = 2$ and $\omega = 0.5$. The three values of $2g^2/\omega = 1.69$, 2.25, and 2.89 correspond to LL, intermediate, and Peierls states, respectively. We find that in all three regions the charge correlations at 1/4 filling are of the form $\cdots 2000 \cdots$.

the charge susceptibility $\chi_{\rho}(2k_F)/N$ to diverge.

Our SSE results show that the HHM at 1/4 filling is in many respects similar to the 1/2 filled case. In Fig. 8 we show $\chi_{\rho}(2k_F)/N$ and $\pi S_{\sigma}(q_1)/q_1$ versus $2g^2/\omega$. We again find two transitions: first a transition to a spin-gapped state, and second the transition to the Peierls state. As at 1/2 filling, the spin gap opens very close to the point where $U_{\text{eff}} = U - 2g^2/\omega = 0$. The phase diagram at 1/4 filling is therefore nearly identical to the phase diagram at 1/2 filling, with LL, intermediate, and Peierls phases. At present we do not have enough SSE data to investigate whether the tricritical point U_m occurs as at 1/2 filling, but in our data at 1/4 filling, we do find that with increasing U g_{c1} and g_{c2} become closer together. This suggests that a tricritical point also exists at 1/4 filling.

At 1/4 filling there are two possible CDW's that are period-4 ($2k_F$). These have charge densities in cartoon form of either $\cdots 1100 \cdots$ or $\cdots 2000 \cdots$, where "1" or "2" indicates a charge density greater than the average density of 0.5 and "0" indicates a charge density less than the average³⁶. The pattern $\cdots 2000 \cdots$ is found in the uncorrelated ($U = 0$) band. In Fig. 9 we plot the real-space charge-charge correlation function $\langle n_i n_j \rangle$ versus distance $|i-j|$ for a range of g 's in the three phases. We find that the charge-charge correlation function peaks for sites separated by four lattice sites, consistent with a CDW state of the $\cdots 2000 \cdots$ form. The strength of the CDW correlations does not greatly change going from the LL to the intermediate phase, but increases rapidly after the Peierls transition. In the $\cdots 2000 \cdots$ CDW, the three small charges are not exactly equal, and the actual charge densities are in sequence large, medium, small, medium (LMSM). This charge pattern coexists with a BOW because L-M and M-S bonds are inequivalent. Fig. 9 shows

that the charge correlations follow this LMSM pattern as expected. We conclude that the pairing at 1/4 filling in the HHM consists of onsite electron pairs as found at 1/2 filling, at least for the small through intermediate U we have currently investigated.

The distinction between these two CDW patterns at 1/4 filling is important because while $\cdots 2000 \cdots$ is related to *onsite* electron pairs, the more extended CDW $\cdots 1100 \cdots$ is related to *nearest-neighbor* pairing. The $\cdots 1100 \cdots$ requires bond-coupled phonons in addition to the Holstein phonons considered here^{36,37}. In addition, the pattern of the BOW (the location of the “strong” bond) coexisting with the $\cdots 1100 \cdots$ CDW also depends on the strength of V ³⁶. If a similar metallic phase exists adjacent to the $\cdots 1100 \cdots$ CDW, it is possible that a region of nearest-neighbor superconducting pairing will be found that may be relevant to real 1/4 filled molecular superconductors.

V. CONCLUSIONS

To summarize, we have presented numerical data for charge and spin correlations of the 1D HHM model at 1/2 and 1/4 filling. We have based our phase diagram on charge and spin susceptibilities, which provide direct indication of phase boundaries with much weaker finite-size effects than previous calculations based on LL exponents¹². We find that the spin gap and Peierls transitions do not occur simultaneously unless U is larger than a critical U_m . For $U < U_m$ as the e-ph coupling is increased from zero, the spin gap opens *before* the Peierls state forms. The intermediate state is metallic with a spin gap but no charge gap, and the transitions to and from the intermediate state are of the KT type. Our physical picture of the intermediate state is that at the spin gap transition (g_{c1}), pairs are formed, but do not order in a Peierls state until the e-ph coupling is further increased. For $U > U_m$, the two transitions merge into a single first-order Mott/Peierls transition. With finite-size calculations we cannot completely discount the possibility of a small charge gap (small compared than the finite-size gap) in the intermediate region. However, further evidence for a lack of a charge gap in the intermediate state is in the charge stiffness data presented in a previous work¹².

The intermediate state deserves some additional dis-

cussion. Considering the possible modification of the LL equations in the presence of retarded e-ph interactions, we find that while this could possibly occur in a form that would agree with Reference 23, the amount renormalization is small ($1/A \sim 0.95$), and probably within finite-size errors in our determination of the transition points. We also do not see any measurable or consistent change in the constant A when comparing $\omega = 0.5$ and $\omega = 1$, which would be expected to change the amount of retardation in the e-ph interaction. If one assumes $1/A < 1$, the size of the intermediate region is actually *enlarged* slightly from what is apparent using the boundary $K_\rho = 1$. We are not able to calculate a value for B in Eq. 23. However, if Eq. 23 is correct for the HHM model with $B < 1$, SS correlations would actually be *enhanced* because of retardation²³.

The second important question is the strength of SS correlations within the intermediate region. In terms of the LL framework, models with $K_\rho > 1$ have dominant superconducting correlations. Indeed, our numerical data appears to show $K_\rho > 1$ in the intermediate region. If we set aside any renormalization of K_ρ , our conclusion based on comparison with the 1D negative- U Hubbard model is that in the intermediate region, K_ρ is *exactly* equal to one. This implies that in the intermediate region that CDW and SS correlations are in fact *exactly degenerate*. This exact degeneracy may not be easily observable in a finite system due to the finite size difficulties near KT transitions. As the SSE method is based on a world-line approach in imaginary time, there is no simple way to measure correlations involving four particles, which would be needed to measure SS correlations directly. Other QMC²⁵ and DMRG²⁴ calculations suggest that while SS and CDW correlations are nearly degenerate in the intermediate region, CDW correlations appear slightly stronger at long range. We however remark that in addition to the logarithmic scaling difficulties, observing metallic behavior in close proximity to a CDW is difficult, and especially in QMC methods based on local updates autocorrelation times may be extremely high for such states. We do find in our method that the autocorrelation time increases close to the Peierls boundary, and suspect similar problems occur in other QMC and DMRG methods.

The authors acknowledge support of American Chemical Society Petroleum Research Fund, and the Department of Energy grant DE-FG02-06ER46315.

* r.t.clay@msstate.edu

¹ T. Ishiguro, K. Yamaji, and G. Saito, *Organic Superconductors* (Springer-Verlag, New York, 1998).

² O. Gunnarsson, Rev. Mod. Phys. **69**, 575 (1997).

³ T. Holstein, Ann. Phys. **8**, 325 (1959).

⁴ J. Hubbard, Proc. R. Soc. Lond. A **276**, 238 (1963).

⁵ R. E. Peierls, *Quantum Theory of Solids* (Clarendon Press, Oxford, 1955).

⁶ E. H. Lieb and F. Y. Wu, Phys. Rev. Lett. **20**, 1445 (1968).

⁷ J. E. Hirsch and E. Fradkin, Phys. Rev. Lett. **49**, 402 (1982).

⁸ J. E. Hirsch and E. Fradkin, Phys. Rev. B **27**, 4302 (1983).

⁹ C. Q. Wu, Q. F. Huang, and X. Sun, Phys. Rev. B **52**, R15683 (1995).

¹⁰ E. Jeckelmann, C. Zhang, and S. R. White, Phys. Rev. B **60**, 7950 (1999).

¹¹ Y. Takada and A. Chatterjee, Phys. Rev. B **67**, 081102R (2003).

¹² R. T. Clay and R. P. Hardikar, Phys. Rev. Lett. **95**, 096401 (2005).

¹³ A. W. Sandvik, J. Phys. A **25**, 3667 (1992).

¹⁴ A. W. Sandvik, Phys. Rev. B **59**, R14157 (1999).

¹⁵ A. W. Sandvik and D. K. Campbell, Phys. Rev. Lett. **83**, 195 (1999).

¹⁶ P. Sengupta, A. W. Sandvik, and D. K. Campbell, Phys. Rev. B **67**, 245103 (2003).

¹⁷ O. F. Syljuasen and A. W. Sandvik, Phys. Rev. E **66**, 046701 (2002).

¹⁸ A. W. Sandvik, R. R. P. Singh, and D. K. Campbell, Phys. Rev. B **56**, 14510 (1997).

¹⁹ P. Sengupta, A. W. Sandvik, and D. K. Campbell, Phys. Rev. B **65**, 155113 (2002).

²⁰ H. J. Schulz, in *Low-Dimensional conductors and superconductors*, edited by D. Jérôme and L. G. Caron (Plenum, New York, 1987), p. 95.

²¹ J. Voit, Rep. Prog. Phys. **58**, 977 (1995).

²² R. T. Clay, A. W. Sandvik, and D. K. Campbell, Phys. Rev. B **59**, 4665 (1999).

²³ D. Loss and T. Martin, Phys. Rev. B **50**, 12160 (1994).

²⁴ M. Tezuka, R. Arita, and H. Aoki, Phys. Rev. Lett. **95**, 226401 (2005).

²⁵ K.-M. Tam, S.-W. Tsai, D. K. Campbell, and A. H. Castro Neto (2006), preprint, cond-mat/0607700.

²⁶ E. Fradkin and J. E. Hirsch, Phys. Rev. B **27**, 1680 (1983).

²⁷ R. J. Bursill, R. H. McKenzie, and C. J. Hamer, Phys. Rev. Lett. **80**, 5607 (1998).

²⁸ L. G. Caron and S. Moukouri, Phys. Rev. Lett. **76**, 4050 (1996).

²⁹ J. W. Cannon and E. Fradkin, Phys. Rev. B **41**, 9435 (1990).

³⁰ J. W. Cannon, R. T. Scalettar, and E. Fradkin, Phys. Rev. B **44**, 5995 (1991).

³¹ J. E. Hirsch, Phys. Rev. Lett. **53**, 2327 (1983).

³² M. Nakamura, J. Phys. Soc. Jpn. **68**, 3123 (2000).

³³ M. Nakamura, Phys. Rev. B **61**, 16377 (2000).

³⁴ L. G. Caron and C. Bourbonnais, Phys. Rev. B **29**, 4230 (1984).

³⁵ J. Hubbard, Phys. Rev. B **17**, 494 (1978).

³⁶ K. C. Ung, S. Mazumdar, and D. Toussaint, Phys. Rev. Lett. **73**, 2603 (1994).

³⁷ R. T. Clay, S. Mazumdar, and D. K. Campbell, Phys. Rev. B **67**, 115121 (2003).